Geochemical Perspectives Letters

Xenon compatibility in magmatic processes: Hadean to current contexts

Q. Chen, C. Sanloup, D. Horlait, G. Shen

Supplementary Information

The Supplementary Information includes:

- Methods
- Tables S-1 and S-2
- Figures S-1 to S-5
- MS Datasheets S-1 to S-7
- Supplementary Information References

Methods

Sample preparation

For olivine/melt partitioning experiments, starting glass (Table S-1) was prepared from reagent grade oxides and carbonates powders to reproduce the composition of lunar magma ocean at the stage of anorthite crystallisation (Sakai *et al.*, 2014). Powders were first ground and decarbonated by slowly heating in a platinum crucible in an atmospheric furnace from room temperature to 1000 °C, run for 10 hours, molten at 1500 °C for 1 hour, and then quenched in water. Recovered glass was crushed into powder again and remolten twice to ensure homogeneity. Xenon doping was done using a gas loading device (Boettcher *et al.*, 1989) to introduce Xe in a platinum capsule previously filled to one third with crushed glass, and brought to 1610 °C and 2.2 GPa for 40 minutes with a piston cylinder press (run PC202, 'Xe-doped glass' in Table S-1). For mass spectrometry analyses, an additional sample was synthesised (run PC265) using as starting composition a previously Xe-doped basaltic glass synthesised similarly to run PC202, recovered, loaded in a new Pt capsule, and brought to 1.3 GPa and 1100 °C for 3 hours to reach the basalt-olivine stability field. PC265 sample experienced the most massive Fe loss, due to the two successive loadings and piston-cylinder runs using two different Pt capsules. For clinopyroxene-feldspar/melt partitioning experiments, the starting sample was obtained from mixing 90 wt. % of previously synthesised glass with 10 wt. % feldspar (labradorite from Spectrum Mine, Plush, Lake Co., Oregon, courtesy of Marie Baïsset).

In situ partitioning measurements

In situ synchrotron experiments were conducted on beamline 16-BM-B at the Advanced Photon Source (Chicago, U.S.A.). High *P-T* conditions were generated using a Paris-Edinburgh press, with cell-assembly

described in Yamada *et al.* (2011). An energy-dispersive X-ray set-up allowed the simultaneous collection of the diffraction and fluorescence signals on coexisting crystals and melt. To constrain the X-ray path length through the sample and preserve the sample cylindrical geometry, diamond capsules (inner diameter of 750 μm) were used and sealed under *P* by platinum-rhodium caps. MgO cylinder surrounding the graphite heater was modified with two boron-epoxy windows to reduce X-ray absorption for both the incident and diffracted X-rays. Temperature was calibrated from power-*T* curve calibrated against melting temperatures of salts (Kono *et al.*, 2014), and *P* was calculated from the cell volume of MgO (Kono *et al.*, 2010). Uncertainties on *P* and *T* are respectively 0.3 GPa and 80 °C. The design of the cell-assembly insures remarkable stability under high *P-T* conditions and a large vertical access to the sample throughout the experiment. At each *P-T* condition, an X-ray radiograph image of the sample was recorded (Fig. S-1), attesting that the whole sample could be probed through the anvil gap. Energy dispersive X-ray (EDX) data were collected on a Ge solid-state detector with slit size defining the X-ray beam of either 50 × 100 μm^2 or 100 × 100 μm^2, with collection time of 1800 s to 6700 s to optimise the signal to noise ratio for the Xe fluorescence peaks. EDX data were collected with the scattering angle (2-θ) at 10.0310 ± 0.0007°, or at 4.0285 ± 0.0005° if overlap of Xe fluorescence and Bragg diffraction peaks occurred at the higher 2-θ value. EDX data were processed by normalising intensities with live time, and slits size if different between datasets. Due to the lack of information on crystal preferential orientation using EDX, it is not possible to calculate crystal fraction from crystalline Bragg peaks area. Instead, EDX spectra collected on MgO at the same *P-T* conditions as crystal-melt equilibrium were taken as background intensity to calculate crystals *vs.* melt fraction from the intensity ratio between baselines from crystal-rich and melt patterns after background subtraction (Fig. S-2). In the case of Cell2, MgO and crystalline spectra have an overlapping baseline, indicating a melt content less than noise, *i.e.* less than 5 %.

Xenon concentrations were calculated from Xe K_α X-ray fluorescence line using the method described in Chen *et al.* (2022), where the absolute intensity of the fluorescence signal, I_i, depends on the following factors (Simabuco and Nascimento Filho, 1994): (1) beam intensity I_i^0, (2) Xe concentration in the sample $[\mathrm{Xe}]_i$, (3) average density ρ_i, (4) volume of the sample probed by the X-ray beam path V_i, (5) absorption by the sample and the surrounding cell-assembly A, and (6) detector sensitivity S as:

$$[\mathrm{Xe}]_i = \frac{I_i}{I_i^0 \times \rho_i \times V_i \times 10^{-A} \times S} \quad \text{(S-1)}$$

The factors I_i^0, A, and S are identical between crystal-rich and melt patterns. For both synchrotron runs, the sample was first fully molten at the targeted *P*, hence cell-assembly deformation between fully molten state and slightly cooled mineral-melt equilibrium state can be neglected, and Equation S-1 can be simplified to:

$$[\mathrm{Xe}]_i = [\mathrm{Xe}]_{\mathrm{fullmelt}} \times \frac{\Lambda_i}{\Lambda_{\mathrm{fullmelt}}} \times \frac{\rho_{\mathrm{fullmelt}}}{\rho_i} \quad \text{(S-2)}$$

with $[\mathrm{Xe}]_{\mathrm{fullmelt}}$ taken as the starting glass Xe content, and Λ the Xe K_α fluorescence peak area. Density of crystals and melts were calculated from (1) the Murnaghan equation of state and the thermal expansion for anorthite (Tribaudino *et al.*, 2010; Angel, 2004), (2) 3rd order Birch-Murnaghan equation of state for olivine (Liu and Li, 2006), (3) the high-*T* Birch-Murnaghan equation of state of diopside (Zhao *et al.*, 1998), and (4) from the 3rd order Birch-Murnaghan equation of state of mantle melts (Agee and Walker, 1988) and the compositional dependence from the ideal mixing model (Lange and Carmichael, 1987).

For datasets containing a mixture of melt and crystals, Xe weight fraction in crystals can be obtained from mass balance calculations:

$$[\mathrm{Xe}]_{\mathrm{c}} = \frac{[\mathrm{Xe}]_i - x_{i,\mathrm{m}}[\mathrm{Xe}]_{\mathrm{melt}}}{(1 - x_{i,\mathrm{m}})} \quad \text{(S-3)}$$

where $x_{i,\mathrm{m}}$ is the melt fraction in pattern *i*, and $[\mathrm{Xe}]_{\mathrm{melt}}$ is taken from the coexisting pure melt pattern.

Textural, chemical, and mineralogical analyses

Recovered sample images were obtained using a Zeiss Ultra 55 field emission scanning electron microscope (SEM), with a working distance of 7.5 mm and a voltage of 20 kV for detection of Xe. Note that samples recovered from present synchrotron experiments are all bubble free at the SEM scale (Fig. S-3). A few Xe submicron bubbles are observed inside olivine crystals from the additional basalt/olivine sample, although rarely. The major elements (Table S-1) of starting glass and recovered samples were determined using a Cameca SX-FIVE electron probe microanalyser (EPMA) on the Camparis platform at Sorbonne University. Accelerating voltage was set to 15 kV, with 5 nA beam current for Na, Ca, Al, Si and 40 nA for Xe. Note that in order to recover the samples from Paris-Edinburgh press experiments, diamond capsules had to be cracked and polished down. Xenon content in the starting glass was measured by EPMA using Xe calibration established following the procedure developed by Montana *et al.* (1993) by measuring the counts for the neighbouring elements, I (CuI) and Cs (CsCl).

Raman spectra were recorded on a JobinYvon Horiba HR460 spectrometer using a single-grating monochromator with 1500 gratings/mm and an argon laser (514.5 nm wavelength) to confirm the mineralogy of recovered samples (Fig. S-4) as obtained from EPMA analyses.

Mass spectrometry analyses

Xenon content on recovered glass pieces from Cell2, and both crystal-rich and glass pieces from run PC265, was measured by mass-spectrometry (Table S-2). Mass spectrometry (MS) measurements were done at the PIAGARA platform (LP2i-Bordeaux). The samples were beforehand weighted using a CAHN/Ventron 21 automatic electro-balance after performing the mandatory daily calibration. Although this electro-balance is precise down to 0.1 µg (for sample below 2 mg), a ±1 µg error is considered to take into account sample contamination or conversely surface erosion by handling.

The MS employed for the analyses is originally a model 1202 of V. G. Micromass 12 (magnetic sector, 60° deflection, and 12 cm radius instrument), incorporating in a small interior volume and customised with a Nier-type source (from a VG3000) and a Cu-Be electron multiplier detector for quantification (integration counting mode). Each sample was placed in an ultra-high vacuum chamber (below 10^{-8} mbar) and a laser was focused on the base of the sample holder (a Mo crucible, previously annealed at circa 2000 °C under vacuum to eliminate any possible Xe contamination). Description of the laser heating setup is reported in (Horlait *et al.*, 2021). A light laser power was first applied for few minutes to bring the sample and base holder at 50–100 °C in order to check for the presence of atmospheric contamination (physical sorption). For all three measured samples (seven fragments in total), no Xe was detected above the usual blank (few 10^5 of each major Xe isotope) after this pre-heating treatment. The sample fragment was then melted by progressively increasing the laser power. A camera is used to monitor sample evolution and the latter is considered melted once its original form changed to a round shape. After the visual observation of melting, the laser power was still conservatively increased by ~10 % and let steady for a few tens of seconds. For the tiniest samples (1 or 4 µg, see Table S-2), laser power obtained when melting larger sample fragments were applied. The evolved gas was treated by hot metallic powders to trap non-noble gases species and thus let only Xe into the MS setup (Horlait *et al.*, 2021). After a rapid estimation of Xe content by MS with a tiny fraction of the gas released from melted samples, the remaining fraction was spiked with a known amount of a monoisotopic ^{131}Xe gas before introduction in the MS. Xenon content from the sample was then deduced from the ^{i}Xe/^{131}Xe intensity ratios measured by MS. This approach allows reducing MS measurements errors to circa 5 % (main sources of errors stem from uncertainties of pipes volumes and spike ^{131}Xe content). As required the FileMaker sheet compiling raw MS measurements are given in MS Datasheets S-1 to S-7. Individual [Xe] values determined by MS and electro-balance measurements are listed in Table S-2.

Supplementary Tables

Table S-1 Chemical analyses of starting and quenched samples (wt. %). Note that Fe loss may have occurred at two stages, during Xe-doping using platinum capsules in piston-cylinder press experiments which is particularly strong for PC265 due to the successive use of two Pt capsules, and during synchrotron experiments due to Pt-Rh caps used to seal diamond capsules.

Sample	Na_2O	FeO	CaO	MgO	SiO_2	Al_2O_3	Totals
Xe-doped glass	–	12.54	13.47	10.44	45.14	17.24	99.22
		(0.25)	(0.26)	(0.18)	(0.59)	(0.16)	(1.15)
Cell2 quenched glass	–	4.88	15.27	13.07	49.08	18.79	101.31
		(0.19)	(0.28)	(0.22)	(0.52)	(0.26)	(0.73)
Cell2 olivine	–	8.81	0.35	51.12	42.26	0.10	102.75
		(0.87)	(0.06)	(1.16)	(0.45)	(0.05)	(1.1)
PC265 quenched glass	–	3.40	13.77	9.82	48.84	21.21	97.21
		(0.11)	(0.18)	(0.12)	(0.35)	(0.28)	(0.66)
PC265 olivine	–	0.42	0.45	55.83	44.09	0.44	101.41
		(0.61)	(0.29)	(0.96)	(0.66)	(0.35)	(0.71)
Cell3 quenched glass	0.95	0.28	14.52	12.16	49.26	19.62)	96.91
	(0.04)	(0.04)	(0.16)	(0.52)	(0.60)	(0.51)	(0.72)
Cell3 anorthite	1.87	0.17	17.30	0.93	48.77	30.47	99.65
	(0.11)	(0.03)	(0.63)	(0.06)	(0.28)	(1.97)	(0.78)
Cell3 diopside	0.18	0.42	14.96	26.91	53.32	9.29	105.34
	(0.04)	(0.36)	(0.97)	(1.13)	(0.090)	(1.15)	(0.41)

Table S-2 Mass spectrometry analyses. Errors on the Xe contents (from the variance of individual measurements) are given in brackets and refer to the last digit(s) of the corresponding value. Weighted averaging of Xe contents were done by pondering each value by the inverse square of its relative error. To better reflect that dispersion of results from a fragment to another presumably comes from samples heterogeneity rather than from Xe content measurements uncertainties, the errors in the last column are calculated from the variance against the average value of the individual Xe content values.

Analysis	Phase	Weight (µg)	Xe content (wt. %)
Cell2, piece 1	glass	57	$1.84(7) \times 10^{-3}$
Cell2, piece 2	glass	65	$1.42(6) \times 10^{-3}$
Cell2	**glass average**		**1.65(15)** $\times 10^{-3}$
PC265, piece 1	glass	16	$8.9(4) \times 10^{-5}$
PC265, piece 2	glass	1	$9.4(4.7) \times 10^{-5}$
PC265, piece 3	glass	18.8	$3.7(2) \times 10^{-4}$
PC265	**glass average**		**1.5(8)** $\times 10^{-4}$
PC265, piece 4	olivine-rich	4	$2.0(6) \times 10^{-2}$
PC265, piece 5	olivine-rich	4	$4.8(1.5) \times 10^{-3}$
PC265	**olivine-rich average**		**1.3(5)** $\times 10^{-2}$

Supplementary Figures

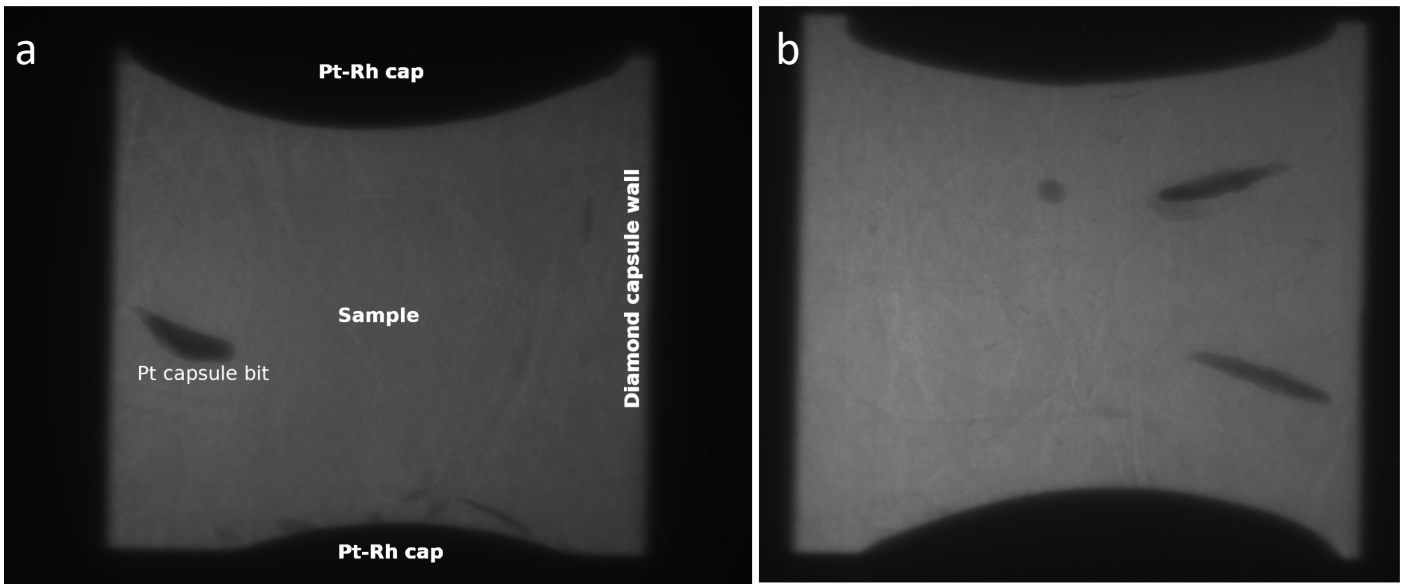

Figure S-1 X-ray radiographs taken at crystals-melt equilibrium and after quenching to room *T* at high *P*. **(a)** olivine/melt experiment (Cell2), **(b)** pyroxene-feldspar/melt experiment (Cell3). Sample width: 750 μm. Thin darker zones on radiographs are Pt bits that fell of the Pt capsule upon retrieving the starting Xe-doped glass.

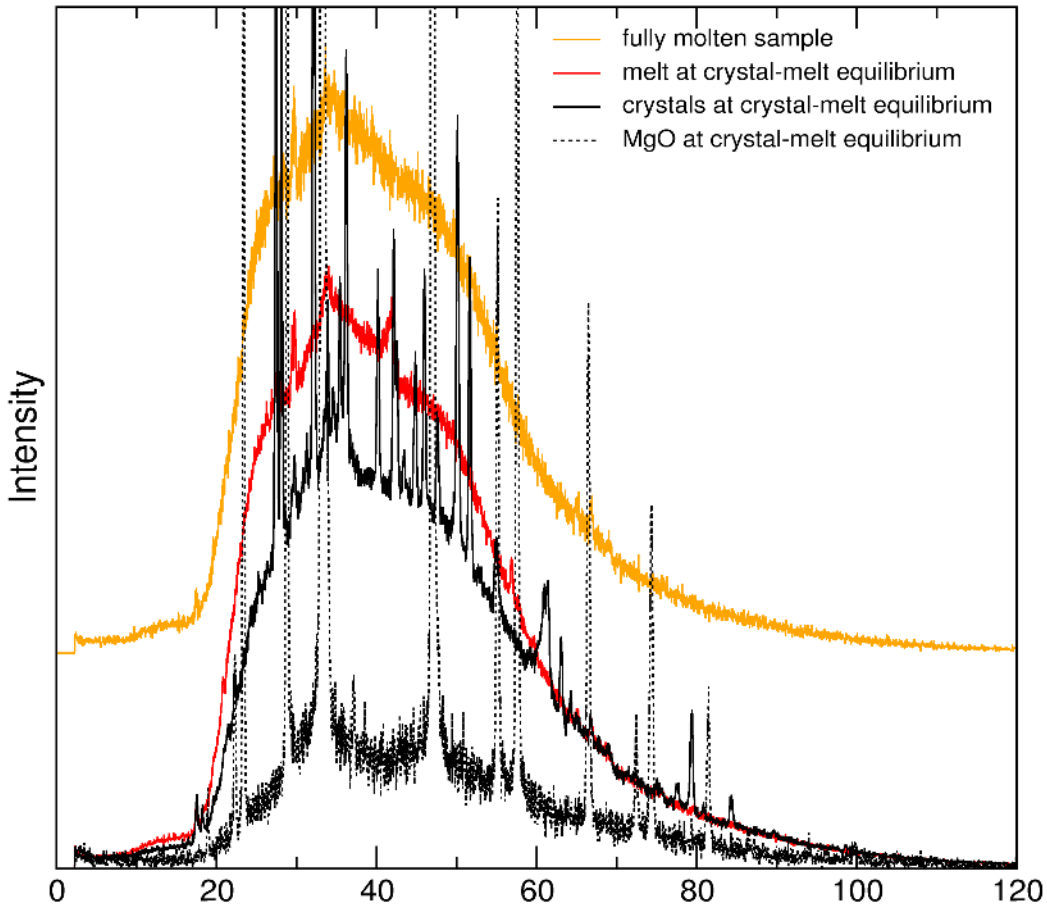

Figure S-2 EDX data collected at 10.031° on anorthite + diopside/melt equilibrium at 1.2 GPa and 1120 °C (Cell3), along with MgO dataset collected at the same *P-T* conditions, and taken as background intensity to calculate crystals *vs.* melt fraction (34(4) % crystals for this dataset) from the intensity ratio between baselines from crystal-rich and melt patterns after background subtraction.

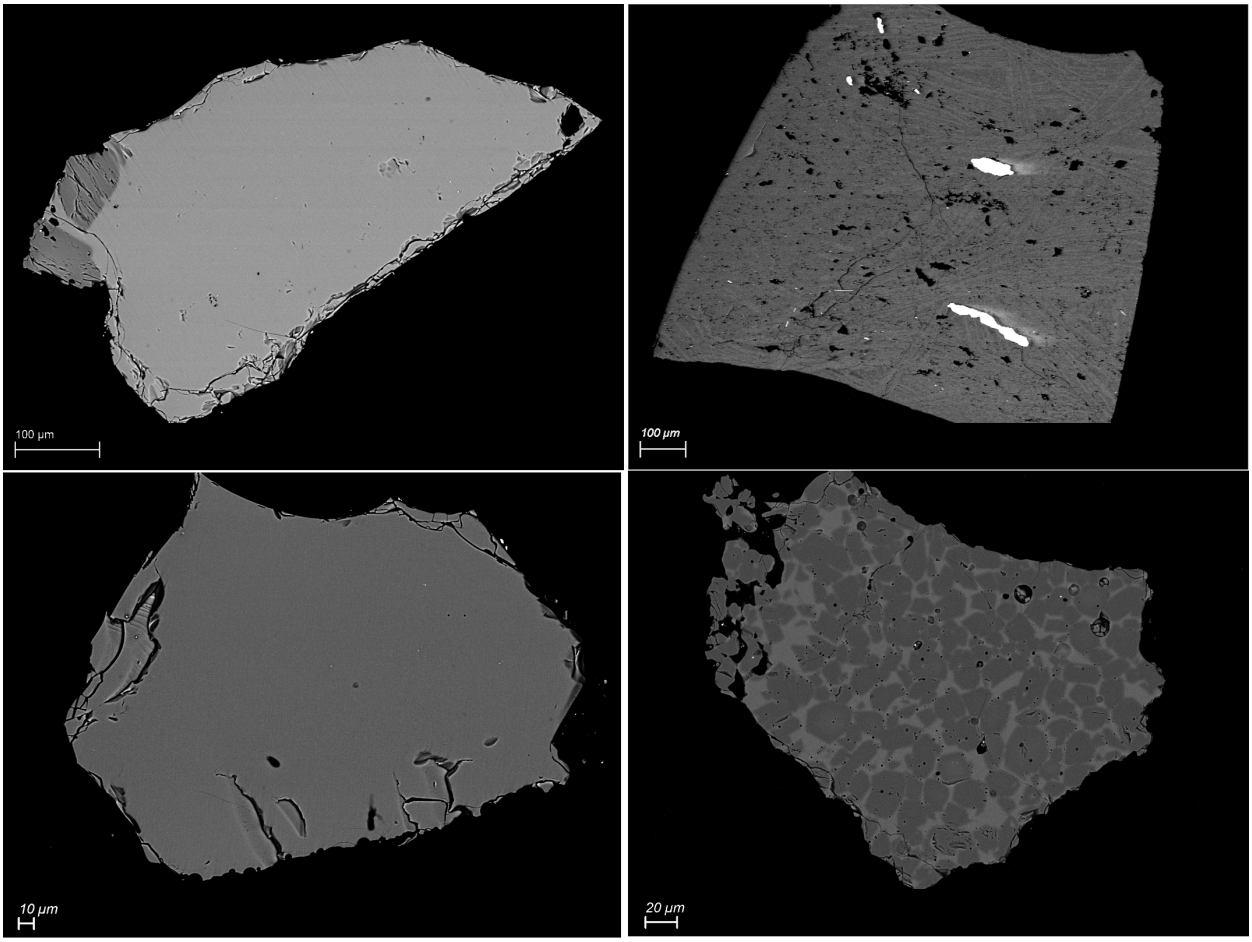

Figure S-3 SEM images of quenched samples. Top left: recovered sample piece from the olivine/melt experiment (Cell2) with two visible olivine crystals. Top right: whole recovered sample from the pyroxene-feldspar/melt experiment (Cell3), with mostly small size crystals and a fully glassy zone on the left hand side; bright zones are Pt bits that fell of the Pt capsule used to synthesise the starting Xe-doped glass. Bottom: sample slices from the olivine/melt additional experiment (PC265) used for mass-spectrometry analyses (pure glass on the left and mostly olivine crystals on the right).

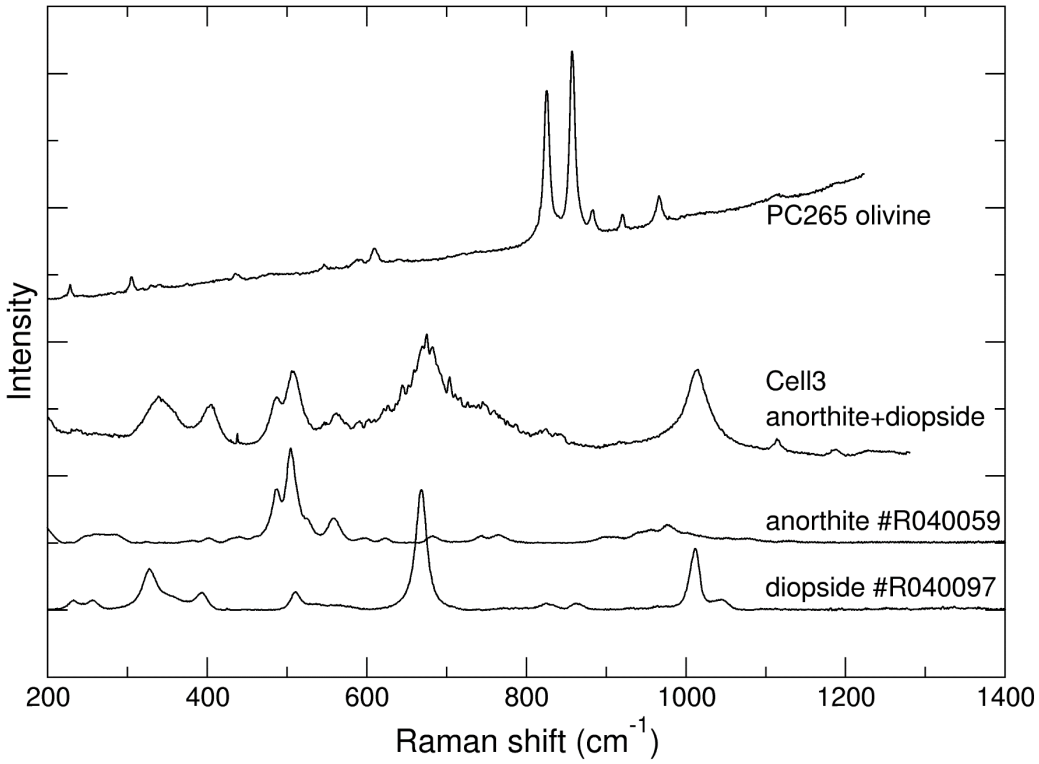

Figure S-4 Raman spectra collected on recovered samples from Cell3 and PC265. Spectra from RRUFF database (Lafuente *et al.*, 2016) are shown for comparison and identification of diopside and anorthite.

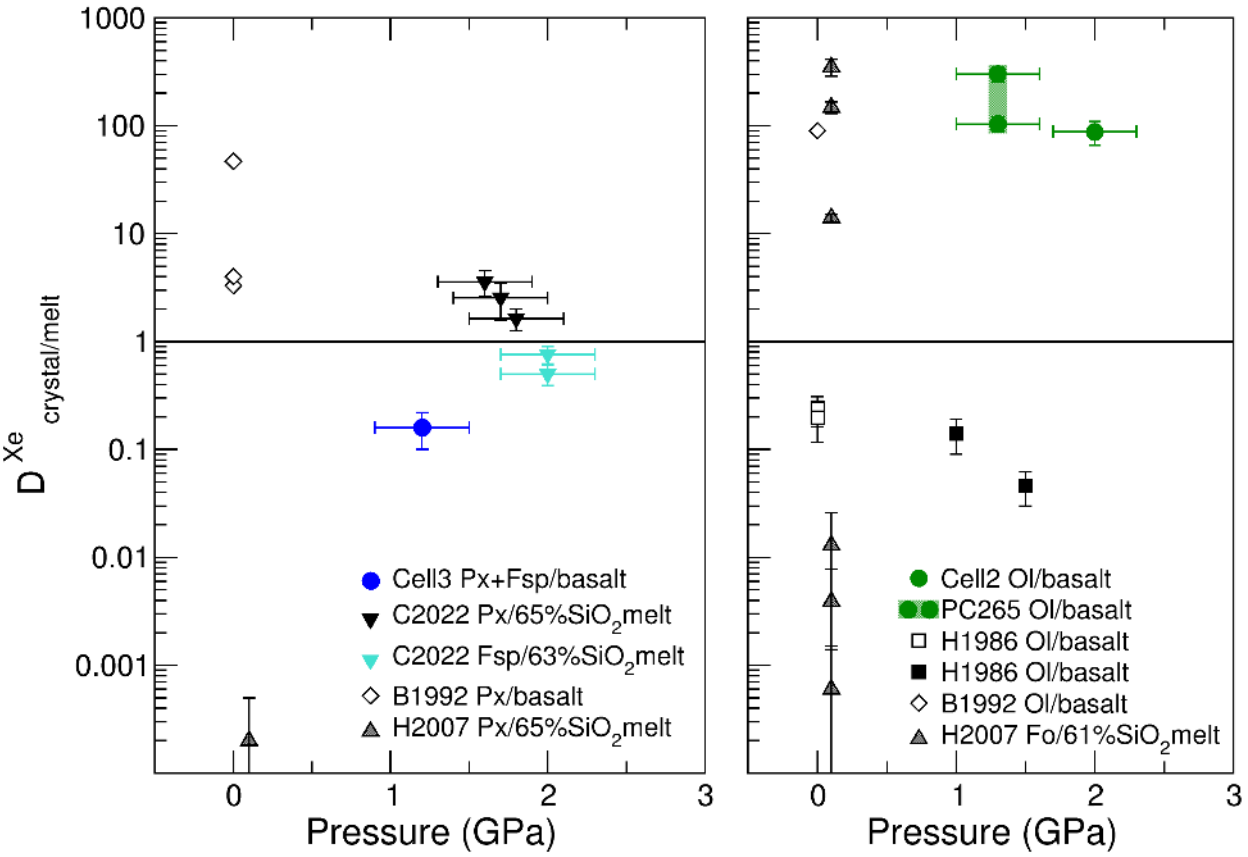

Figure S-5 Xenon crystal/melt partition coefficients as a function of pressure (left, pyroxene-feldspar/melt; right, olivine/melt). Data abbreviations: H1986, Hiyagon and Ozima (1986); B1992, Broadhurst *et al.* (1992); H2007, Heber *et al.* (2007); C2022, Chen *et al.* (2022); PC265, Cell2, and Cell3 are data from this study (Table 2). Note that Heber *et al.* (2007) discarded all values above unity due to the observation of gas bubbles in crystals.

Supplementary MS datasheets

Datasheet S-1 Annotated datasheet displaying the mixing of the Xe gas obtained from the melting of the sample "Cell2, piece 1" (see Table S-2) mixed with a precisely known ^{131}Xe monoisotopic reference gas. As explained in the previous section of this document, the measurement by MS of the ^{i}Xe/^{131}Xe ratios in the "sample + reference" gas mix allows to precisely deduce the Xe amount in the sample, without having to determine the sensitivity of the MS.

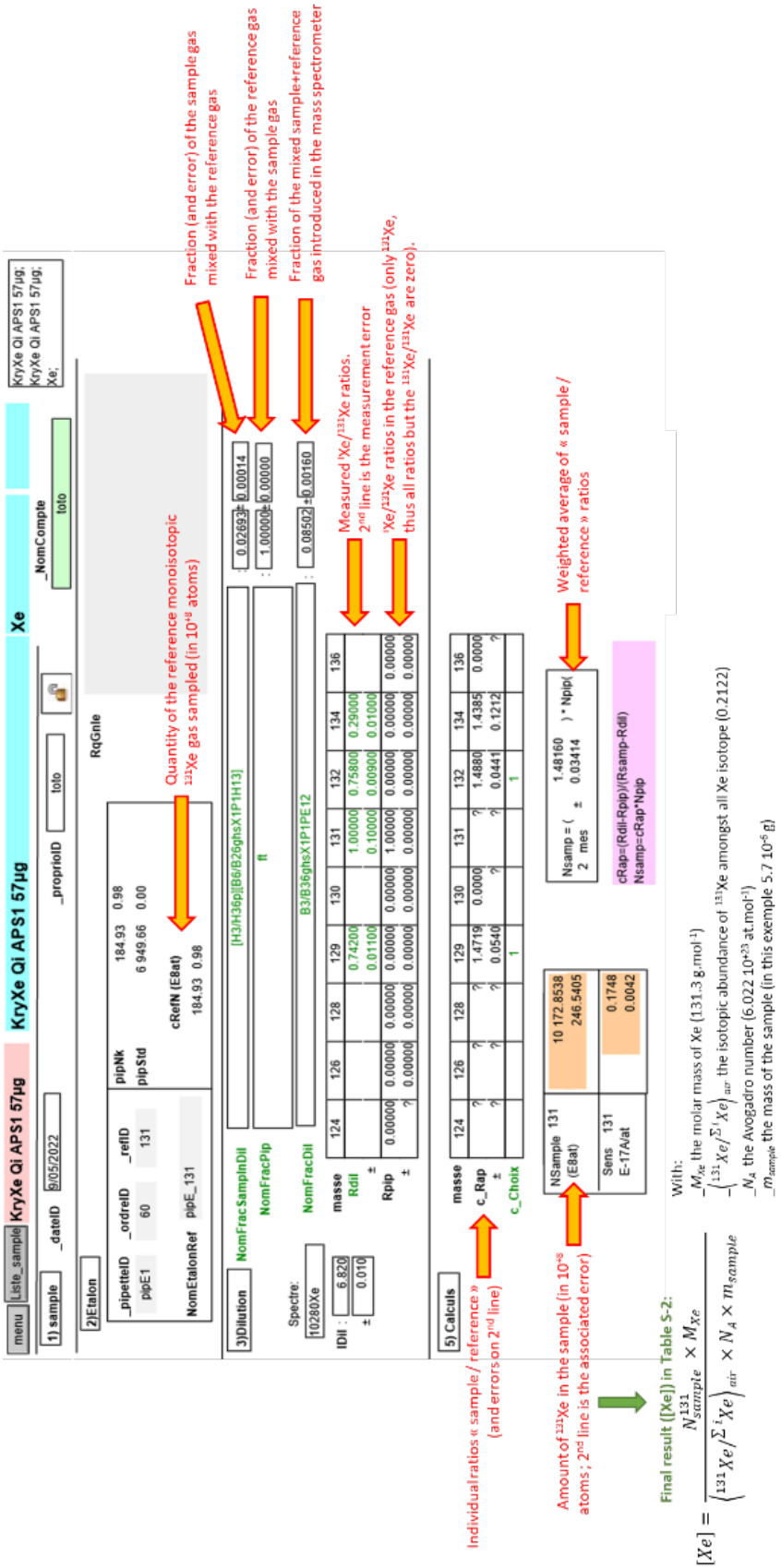

Datasheet S-2 MS datasheet for sample "Cell2, piece 2" (see Table S-2). For details, refer to annotated Datasheet S-1 and its caption.

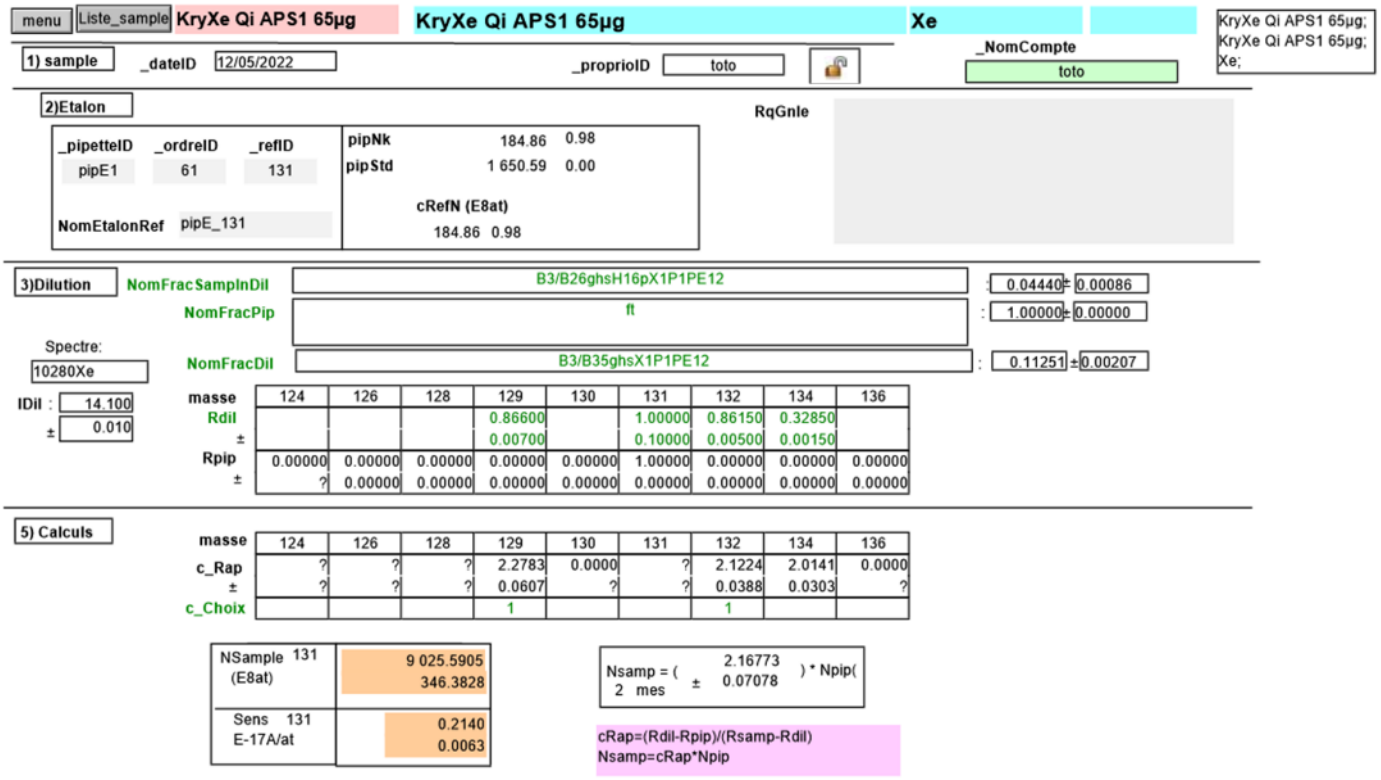

menu | Liste_sample | KryXe Qi APS1 65µg | KryXe Qi APS1 65µg | Xe | KryXe Qi APS1 65µg; KryXe Qi APS1 65µg; Xe;

1) sample _dateID 12/05/2022 _proprioID toto _NomCompte toto

2)Etalon RqGnle

_pipetteID	_ordreID	_refID
pipE1	61	131

NomEtalonRef pipE_131

pipNk 184.86 0.98
pipStd 1 650.59 0.00
cRefN (E8at) 184.86 0.98

3)Dilution NomFracSampInDil B3/B26ghsH16pX1P1PE12 : 0.04440 ± 0.00086
NomFracPip ft : 1.00000 ± 0.00000
Spectre: 10280Xe NomFracDil B3/B35ghsX1P1PE12 : 0.11251 ± 0.00207
IDil : 14.100 ± 0.010

masse	124	126	128	129	130	131	132	134	136
Rdil				0.86600		1.00000	0.86150	0.32850	
±				0.00700		0.10000	0.00500	0.00150	
Rpip	0.00000	0.00000	0.00000	0.00000	0.00000	1.00000	0.00000	0.00000	0.00000
±	?	0.00000	0.00000	0.00000	0.00000	0.00000	0.00000	0.00000	0.00000

5) Calculs

masse	124	126	128	129	130	131	132	134	136
c_Rap	?	?	?	2.2783	0.0000	?	2.1224	2.0141	0.0000
±	?	?	?	0.0607	?	?	0.0388	0.0303	?
c_Choix				1			1		

NSample 131 (E8at) 9 025.5905 346.3828
Sens 131 E-17A/at 0.2140 0.0063

Nsamp = (2.16773 ± 0.07078) * Npip(2 mes

cRap=(Rdil-Rpip)/(Rsamp-Rdil)
Nsamp=cRap*Npip

Datasheet S-3 MS datasheet for sample "PC265, piece 4" (see Table S-2). For details, refer to annotated Datasheet S-1 and its caption.

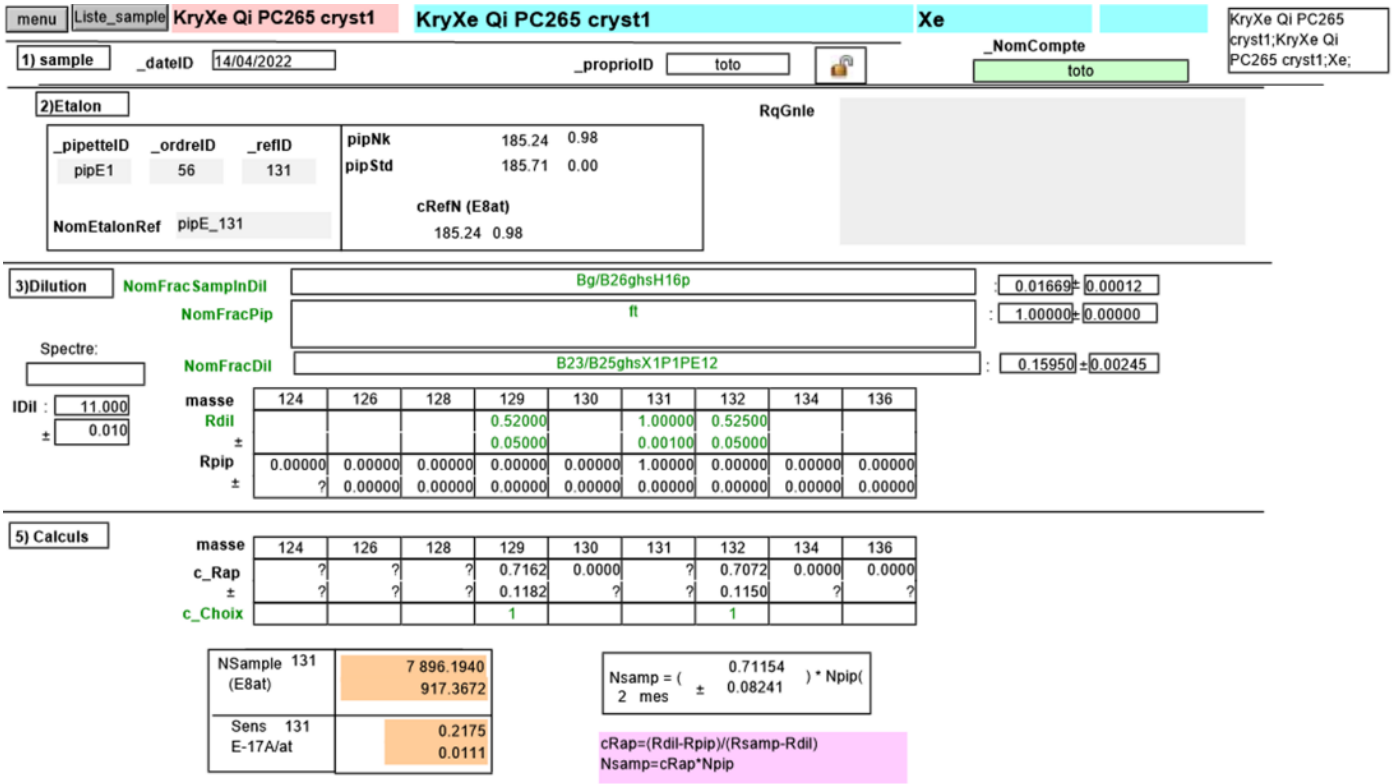

menu | Liste_sample | KryXe Qi PC265 cryst1 | KryXe Qi PC265 cryst1 | Xe | KryXe Qi PC265 cryst1;KryXe Qi PC265 cryst1;Xe;

1) sample _dateID 14/04/2022 _proprioID toto _NomCompte toto

2)Etalon RqGnle

_pipetteID	_ordreID	_refID
pipE1	56	131

NomEtalonRef pipE_131

pipNk 185.24 0.98
pipStd 185.71 0.00
cRefN (E8at) 185.24 0.98

3)Dilution NomFracSampInDil Bg/B26ghsH16p : 0.01669 ± 0.00012
NomFracPip ft : 1.00000 ± 0.00000
Spectre: NomFracDil B23/B25ghsX1P1PE12 : 0.15950 ± 0.00245
IDil : 11.000 ± 0.010

masse	124	126	128	129	130	131	132	134	136
Rdil				0.52000		1.00000	0.52500		
±				0.05000		0.00100	0.05000		
Rpip	0.00000	0.00000	0.00000	0.00000	0.00000	1.00000	0.00000	0.00000	0.00000
±	?	0.00000	0.00000	0.00000	0.00000	0.00000	0.00000	0.00000	0.00000

5) Calculs

masse	124	126	128	129	130	131	132	134	136
c_Rap	?	?	?	0.7162	0.0000	?	0.7072	0.0000	0.0000
±	?	?	?	0.1182	?	?	0.1150	?	?
c_Choix				1			1		

NSample 131 (E8at) 7 896.1940 917.3672
Sens 131 E-17A/at 0.2175 0.0111

Nsamp = (0.71154 ± 0.08241) * Npip(2 mes

cRap=(Rdil-Rpip)/(Rsamp-Rdil)
Nsamp=cRap*Npip

Datasheet S-4 MS datasheet for sample "PC265, piece 5" (see Table S-2). For details, refer to annotated Datasheet S-1 and its caption.

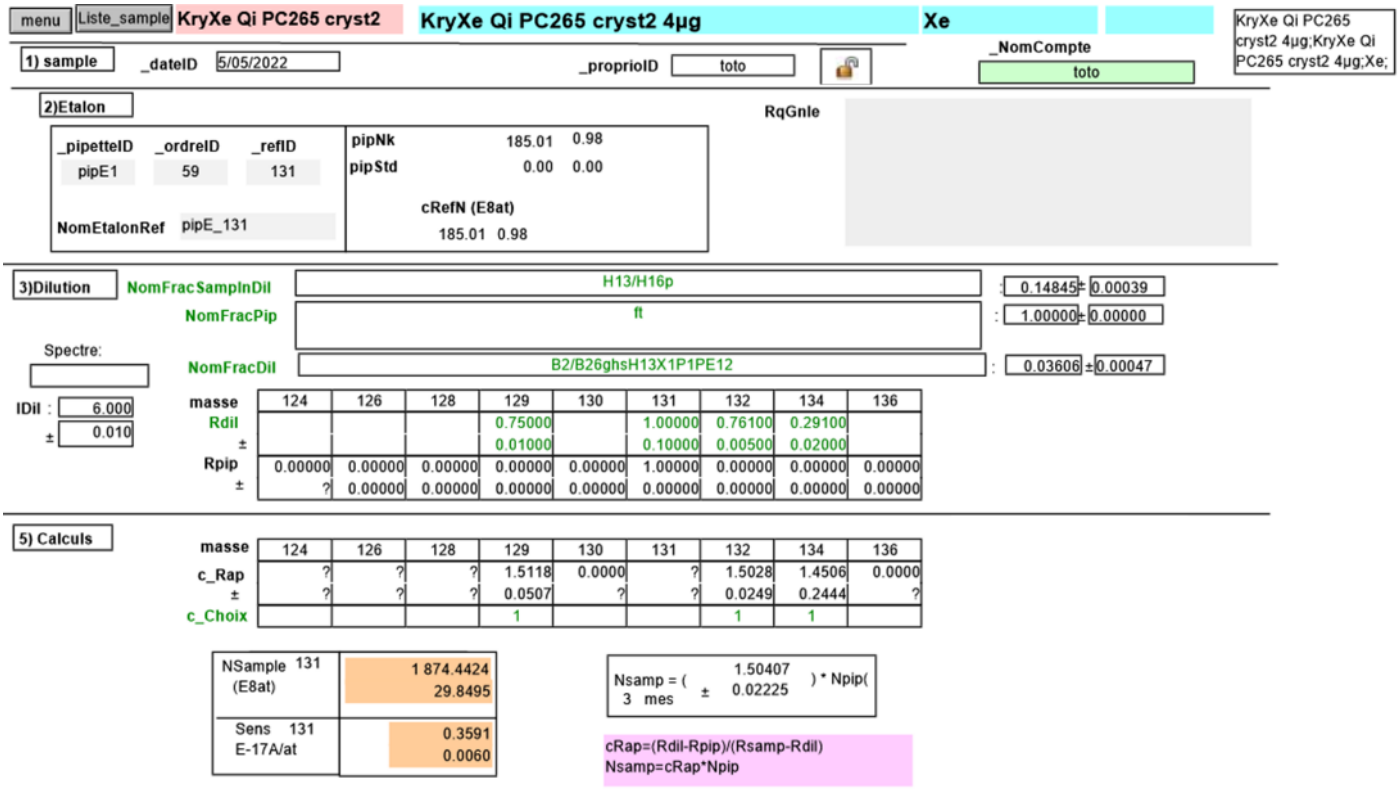

menu | Liste_sample | KryXe Qi PC265 cryst2 | KryXe Qi PC265 cryst2 4µg | Xe | KryXe Qi PC265 cryst2 4µg;KryXe Qi PC265 cryst2 4µg;Xe;

1) sample | _dateID 5/05/2022 | _proprioID toto | _NomCompte toto

2)Etalon | RqGnle

_pipetteID	_ordreID	_refID
pipE1	59	131

NomEtalonRef pipE_131

pipNk	185.01	0.98
pipStd	0.00	0.00

cRefN (E8at): 185.01 0.98

3)Dilution | NomFracSampInDil: H13/H16p : 0.14845 ± 0.00039 | NomFracPip: ft : 1.00000 ± 0.00000 | NomFracDil: B2/B26ghsH13X1P1PE12 : 0.03606 ± 0.00047

Spectre:

IDil : 6.000 ± 0.010

masse	124	126	128	129	130	131	132	134	136
Rdil				0.75000		1.00000	0.76100	0.29100	
±				0.01000		0.10000	0.00500	0.02000	
Rpip	0.00000	0.00000	0.00000	0.00000	0.00000	1.00000	0.00000	0.00000	0.00000
±	?	0.00000	0.00000	0.00000	0.00000	0.00000	0.00000	0.00000	0.00000

5) Calculs

masse	124	126	128	129	130	131	132	134	136
c_Rap	?	?	?	1.5118	0.0000	?	1.5028	1.4506	0.0000
±	?	?	?	0.0507	?	?	0.0249	0.2444	?
c_Choix				1			1	1	

NSample 131 (E8at)	1 874.4424
	29.8495
Sens 131 E-17A/at	0.3591
	0.0060

Nsamp = (1.50407 ± 0.02225) * Npip(3 mes

cRap=(Rdil-Rpip)/(Rsamp-Rdil)
Nsamp=cRap*Npip

Datasheet S-5 MS datasheet for sample "PC265, piece 1" (see Table S-2). For details, refer to annotated Datasheet S-1 and its caption.

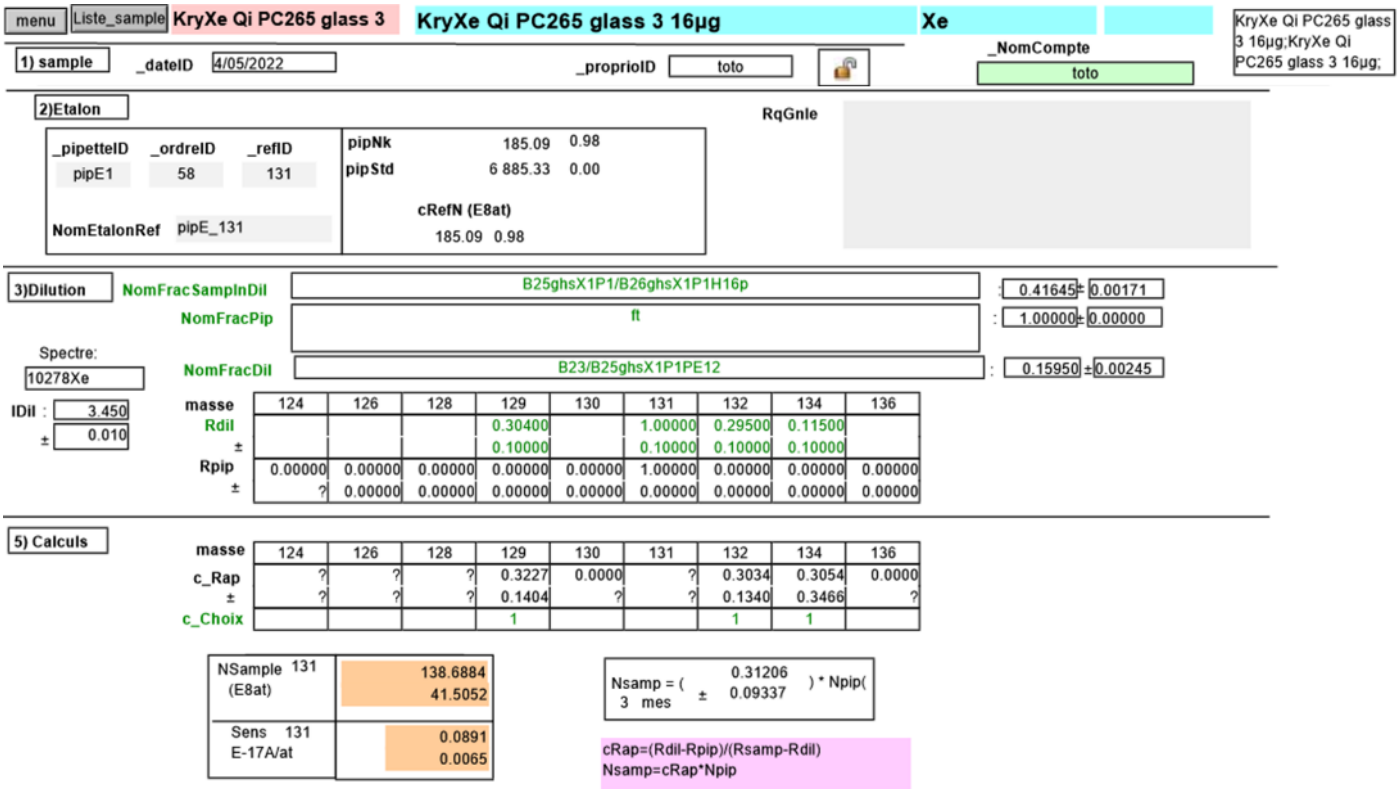

menu | Liste_sample | KryXe Qi PC265 glass 3 | KryXe Qi PC265 glass 3 16µg | Xe | KryXe Qi PC265 glass 3 16µg;KryXe Qi PC265 glass 3 16µg;

1) sample | _dateID 4/05/2022 | _proprioID toto | _NomCompte toto

2)Etalon | RqGnle

_pipetteID	_ordreID	_refID
pipE1	58	131

NomEtalonRef pipE_131

pipNk	185.09	0.98
pipStd	6 885.33	0.00

cRefN (E8at): 185.09 0.98

3)Dilution | NomFracSampInDil: B25ghsX1P1/B26ghsX1P1H16p : 0.41645 ± 0.00171 | NomFracPip: ft : 1.00000 ± 0.00000 | NomFracDil: B23/B25ghsX1P1PE12 : 0.15950 ± 0.00245

Spectre: 10278Xe

IDil : 3.450 ± 0.010

masse	124	126	128	129	130	131	132	134	136
Rdil				0.30400		1.00000	0.29500	0.11500	
±				0.10000		0.10000	0.10000	0.10000	
Rpip	0.00000	0.00000	0.00000	0.00000	0.00000	1.00000	0.00000	0.00000	0.00000
±	?	0.00000	0.00000	0.00000	0.00000	0.00000	0.00000	0.00000	0.00000

5) Calculs

masse	124	126	128	129	130	131	132	134	136
c_Rap	?	?	?	0.3227	0.0000	?	0.3034	0.3054	0.0000
±	?	?	?	0.1404	?	?	0.1340	0.3466	?
c_Choix				1			1	1	

NSample 131 (E8at)	138.6884
	41.5052
Sens 131 E-17A/at	0.0891
	0.0065

Nsamp = (0.31206 ± 0.09337) * Npip(3 mes

cRap=(Rdil-Rpip)/(Rsamp-Rdil)
Nsamp=cRap*Npip

Datasheet S-6 MS datasheet for sample "PC265, piece 2" (see Table S-2). For details, refer to annotated Datasheet S-1 and its caption.

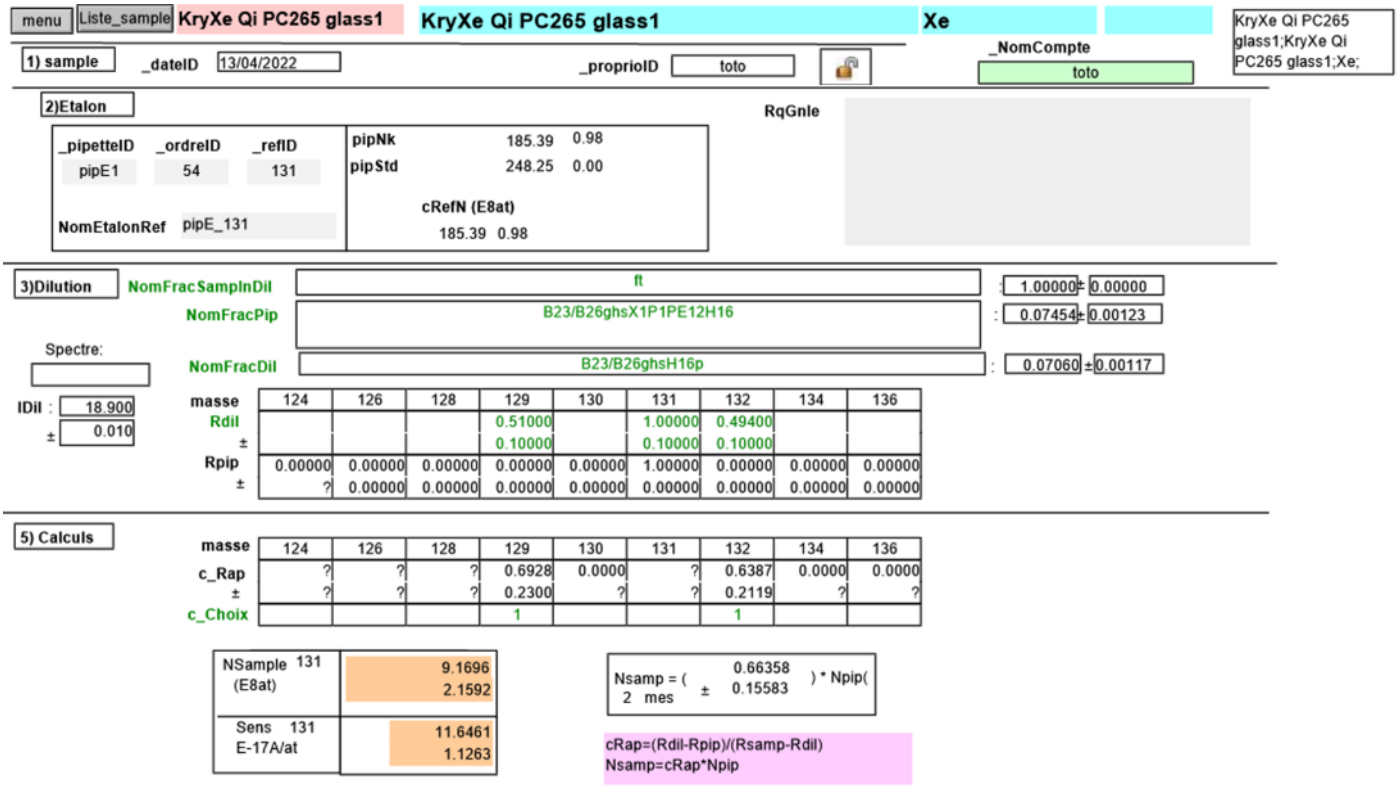

Datasheet S-7 MS datasheet for sample "PC265, piece 3" (see Table S-2). For details, refer to annotated Datasheet S-1 and its caption.

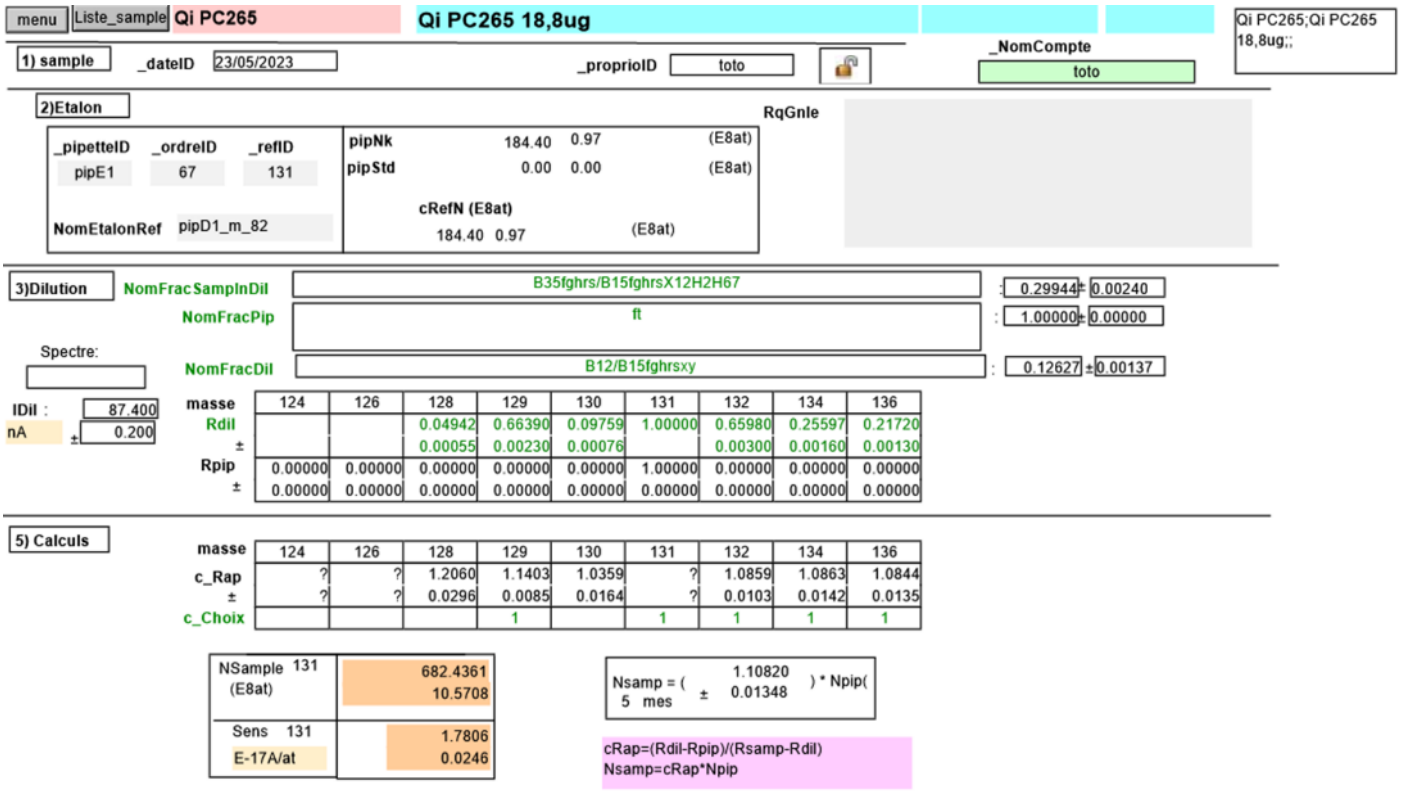

Supplementary Information References

Agee, C.B., Walker, D. (1988) Static compression and olivine flotation in ultrabasic silicate liquid. *Journal of Geophysical Research: Solid Earth* 93, 3437–3449. https://doi.org/10.1029/JB093iB04p03437

Angel, R.J. (2004) Equations of state of Plagioclase Feldspars. *Contributions to Mineralogy and Petrology* 146, 506–512. https://doi.org/10.1007/s00410-003-0515-5

Boettcher, S.L., Qiti, G., Montana, A. (1989) A simple device for loading gases in high-pressure experiments. *American Mineralogist* 74, 1383–1384. http://www.minsocam.org/ammin/AM74/AM74_1383.pdf

Broadhurst, C.L., Drake, M.J., Hagee, B.E., Bernatowicz, T.J. (1992) Solubility and partitioning of Ne, Ar, Kr, and Xe in minerals and synthetic basaltic melts. *Geochimica et Cosmochimica Acta* 56, 709–723. https://doi.org/10.1016/0016-7037(92)90092-W

Chen, Q., Sanloup, C., Bureau, H., Rzeplinski, I., Glazyrin, K., Farla, R. (2022) Probing the partitioning behaviour of Xe using *in situ* X-ray synchrotron techniques at high *P–T* conditions. *High Pressure Research* 42, 318–335. https://doi.org/10.1080/08957959.2022.2144290

Heber, V.S., Brooker, R.A., Kelley, S.P., Wood, B.J. (2007) Crystal-melt partitioning of noble gases (helium, neon, argon, krypton, and xenon) for olivine and clinopyroxene. *Geochimica et Cosmochimica Acta* 71, 1041–1061. https://doi.org/10.1016/j.gca.2006.11.010

Hiyagon, H., Ozima, M. (1986) Partition of noble gases between olivine and basalt melt. *Geochimica et Cosmochimica Acta* 50, 2045–2057. https://doi.org/10.1016/0016-7037(86)90258-9

Horlait, D., Faure, R., Thomas, B.A., Devert, N., Amany, M.-L., Carlot, G., Gilabert, E. (2021) A new thermo-desorption laser-heating setup for studying noble gases diffusion and release from materials at high temperatures. *Review of Scientific Instruments* 92, 124102. https://doi.org/10.1063/5.0068858

Kono, Y., Irifune, T., Higo, Y., Inoue, T., Barnhoorn, A. (2010) *P–V–T* relation of MgO derived by simultaneous elastic wave velocity and in situ X-ray measurements: A new pressure scale for the mantle transition region. *Physics of the Earth and Planetary Interiors* 183, 196–211. https://doi.org/10.1016/j.pepi.2010.03.010

Kono, Y., Park, C., Kenney-Benson, C., Shen, G., Wang, Y. (2014) Toward comprehensive studies of liquids at high pressures and high temperatures: Combined structure, elastic wave velocity, and viscosity measurements in the Paris-Edinburgh cell. *Physics of the Earth and Planetary Interiors* 228, 269–280. https://doi.org/10.1016/j.pepi.2013.09.006

Lafuente, B., Downs, R.T., Yang, H., Stone, N. (2016) 1. The power of databases: The RRUFF project. In: Armbruster, T., Danisi, R.M. (Eds.) *Highlights in Mineralogical Crystallography.* De Gruyter, Berlin, 1-30. https://doi.org/10.1515/9783110417104-003

Lange, R.A., Carmichael, I.S.E. (1987) Densities of Na_2O-K_2O-CaO-MgO-FeO-Fe_2O_3-Al_2O_3-TiO_2-SiO_2 liquids: New measurements and derived partial molar properties. *Geochimca et Cosmochimica Acta* 51, 2931–2946. https://doi.org/10.1016/0016-7037(87)90368-1

Liu, W., Li, B. (2006) Thermal equation of state of $(Mg_{0.9}Fe_{0.1})_2SiO_4$ olivine. *Physics of the Earth and Planetary Interiors* 157, 188–195. https://doi.org/10.1016/j.pepi.2006.04.003

Montana, A., Guo, Q., Boettcher, S., White, B.S., Brearley, M. (1993) Xe and Ar in high-pressure silicate liquids. *American Mineralogist* 78, 1135–1142. http://www.minsocam.org/ammin/AM78/AM78_1135.pdf

Sakai, R., Nagahara, H., Ozawa, K., Tachibana, S. (2014) Composition of the lunar magma ocean constrained by the conditions for the crust formation. *Icarus* 229, 45–56. https://doi.org/10.1016/j.icarus.2013.10.031

Simabuco, S.M., Nascimento Filho, V.F. (1994) Quantitative analysis by energy dispersive X-ray fluorescence by the transmission method applied to geological samples. *Scientia Agricola* 51, 197–206. https://doi.org/10.1590/S0103-90161994000200001

Tribaudino, M., Angel, R.J., Cámara, F., Nestola, F., Pasqual, D., Margiolaki, I. (2010) Thermal expansion of plagioclase feldspars. *Contributions to Mineralogy and Petrology* 160, 899–908. https://doi.org/10.1007/s00410-010-0513-3

Yamada, A., Wang, Y., Inoue, T., Yang, W., Park, C., Yu, T., Shen, G. (2011) High-pressure x-ray diffraction studies on the structure of liquid silicate using a Paris–Edinburgh type large volume press. *Review of Scientific Instruments* 82, 015103. https://doi.org/10.1063/1.3514087

Zhao, Y., Von Dreele, R.B., Zhang, J.Z., Weidner, D.J. (1998) Thermoelastic Equation of State of Monoclinic Pyroxene: $CaMgSi_2O_6$ Diopside. *The Review of High Pressure Science and Technology* 7, 25–27. https://doi.org/10.4131/JSHPREVIEW.7.25